

Catalysis

Interaction of Hydrogen with Ceria: Hydroxylation, Reduction, and Hydride Formation on the Surface and in the Bulk

Zhaorui Li⁺,^[a] Kristin Werner⁺,^[b] Lu Chen⁺,^[c] Aiping Jia,^[a, d] Kun Qian,^[a] Jian-Qiang Zhong,^[b] Rui You,^[a] Lihui Wu,^[e] Liyuan Zhang,^[a] Haibin Pan,^[e] Xin-Ping Wu,^{*[c]} Xue-Qing Gong,^[c] Shamil Shaikhutdinov,^{*[b]} Weixin Huang,^{*[a, f]} and Hans-Joachim Freund^[b]

Abstract: The study reports the first attempt to address the interplay between surface and bulk in hydride formation in ceria (CeO₂) by combining experiment, using surface sensitive and bulk sensitive spectroscopic techniques on the two sample systems, i.e., CeO₂(111) thin films and CeO₂ powders, and theoretical calculations of CeO₂(111) surfaces with oxygen vacancies (O_v) at the surface and in the bulk. We show that, on a stoichiometric CeO₂(111) surface, H₂ dissociates and forms surface hydroxyls (OH). On the pre-reduced CeO_{2-x} samples, both films and powders, hydroxyls and hydrides (Ce–H) are formed on the surface as well as in the bulk, accompanied by the Ce³⁺ ↔ Ce⁴⁺ redox reaction. As the O_v concentration increases, hydroxyl is destabilized and

hydride becomes more stable. Surface hydroxyl is more stable than bulk hydroxyl, whereas bulk hydride is more stable than surface hydride. The surface hydride formation is the kinetically favorable process at relatively low temperatures, and the resulting surface hydride may diffuse into the bulk region and be stabilized therein. At higher temperatures, surface hydroxyls can react to produce water and create additional oxygen vacancies, increasing its concentration, which controls the H₂/CeO₂ interaction. The results demonstrate a large diversity of reaction pathways, which have to be taken into account for better understanding of reactivity of ceria-based catalysts in a hydrogen-rich atmosphere.

Introduction

Interaction of hydrogen with metal oxides is intimately involved in many important processes, from H₂ storage to thermal, photo- and electro-catalysis.^[1] It exhibits complex behavior,^[2] including homolytic dissociation at two oxygen sites, thermodynamically favored for readily reducible oxides leading to two hydroxyl (OH) groups and the concomitant reduction of two surface metal cations, and heterolytic dissociation at metal and oxygen sites primarily occurring on oxides difficult

to reduce. The process may involve the migration of H atoms into the sub-surface region and the bulk to form hydroxyl and hydride (H⁻) species therein.

Beyond this, the interaction of H₂ with ceria (CeO₂) has recently received much attention because ceria, widely used as oxidation catalysts, demonstrate the potential as a selective catalyst for alkyne semi-hydrogenation reactions.^[3] It is assumed that H₂ undergoes dissociation forming two surface OH groups.^[4] The resulting OH groups react to produce water at elevated temperatures, creating oxygen vacancies (O_v). Density

[a] Z. Li,⁺ A. Jia, Dr. K. Qian, Dr. R. You, L. Zhang, Prof. W. Huang
 Hefei National Laboratory for Physical Sciences at Microscale
 Key Laboratory of Surface and Interface Chemistry and Energy Catalysis
 of Anhui Higher Education Institutes, CAS Key Laboratory of Materials
 for Energy Conversion and Department of Chemical Physics
 University of Science and Technology of China, Hefei 230026 (P. R. China)
 E-mail: huangwx@ustc.edu.cn

[b] Dr. K. Werner,⁺ Dr. J.-Q. Zhong, Dr. S. Shaikhutdinov, Prof. Dr. H.-J. Freund
 Fritz-Haber-Institut der Max-Planck Gesellschaft
 Faradayweg 4–6, Berlin 14195 (Germany)
 E-mail: shaikhutdinov@fhi-berlin.mpg.de


[c] L. Chen,⁺ Prof. Dr. X.-P. Wu, Prof. Dr. X.-Q. Gong
 Key Laboratory for Advanced Materials and Joint International Research
 Laboratory for Precision Chemistry and Molecular Engineering, Feringa
 Nobel Prize Scientist Joint Research Center, Centre for Computational
 Chemistry and Research Institute of Industrial Catalysis, School of
 Chemistry and Molecular Engineering, East China University of Science
 and Technology, 130 Meilong Road, Shanghai, 200237 (P. R. China)
 E-mail: xpwu@ecust.edu.cn


[d] A. Jia
 Key Laboratory of the Ministry of Education for Advanced Catalysis
 Materials, Institute of Physical Chemistry, Zhejiang Normal University
 Jinhua 321004 (P. R. China)

[e] Dr. L. Wu, Dr. H. Pan
 National Synchrotron Radiation Laboratory, University of
 Science and Technology of China, Hefei 230029 (P. R. China)

[f] Prof. W. Huang
 Dalian National Laboratory for Clean Energy, Dalian 116023 (P. R. China)

[*] These authors contributed equally to this work.

 Supporting information and the ORCID identification number(s) for the author(s) of this article can be found under:
<https://doi.org/10.1002/chem.202005374>

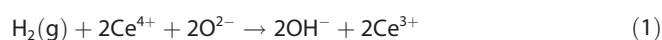
 © 2020 The Authors. Chemistry - A European Journal published by Wiley-VCH GmbH. This is an open access article under the terms of the Creative Commons Attribution Non-Commercial NoDerivs License, which permits use and distribution in any medium, provided the original work is properly cited, the use is non-commercial and no modifications or adaptations are made.

functional theory (DFT) calculations showed that the homolytic dissociation of H₂ at two oxygen sites is thermodynamically favored on fully oxidized, stoichiometric CeO₂(111) surface.^[5] However, the calculations also suggested a heterolytic H₂ dissociation to be kinetically favored on this surface to form a Ce–H and a OH species.^[6] The resulting Ce–H species further evolve to the thermodynamically more stable OH species, accompanied by the reduction of Ce⁴⁺ into Ce³⁺.

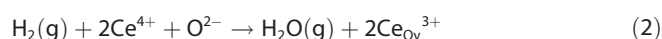
Oxygen vacancies on a ceria surface have been shown, both theoretically and experimentally, to strongly affect the H₂–CeO₂ interaction. The oxygen vacancies can even be formed in situ during the reaction, e.g., by desorption of water via recombination of surface OHs. Theoretical calculations indicated that the stability of Ce–H species resulting from heterolytic H₂ dissociation is enhanced on reduced, i.e., O_v-containing ceria surfaces.^[7] Experimentally, surface oxygen vacancies on CeO₂ were observed to affect the reactivity of surface hydroxyls by suppressing the water production pathway and promoting the H₂ production pathway.^[8] In addition, the processes may be influenced by oxygen vacancy diffusion, as water formation and the accompanied oxygen vacancy formation happen on the surface. According to DFT calculations,^[9] both, vacancy formation and diffusion, are rather independent of surface orientation. Using inelastic neutron scattering spectroscopy, Wu et al.^[10] first reported the direct spectroscopic evidence for the formation of Ce–H species upon H₂ dissociation over ceria powder naturally containing oxygen vacancies. Werner et al.^[11] observed that H₂ dissociation on a fully oxidized CeO₂(111) thin film surface forms hydroxyl species, primarily located at the surface, while on the reduced CeO_{2-x}(111) thin films Ce–H species were also found in appreciable quantities below the surface indicating that the absorption of hydrogen leads to the formation of O_v-stabilized hydride species in the bulk. Furthermore, H₂ adsorption at room temperature was shown to lead to the oxidation of Ce³⁺ in both CeO_{2-x}(111) thin films and CeO_{2-x} powders to Ce⁴⁺,^[12] demonstrating the formation of more Ce–H hydride species at the Ce³⁺–O_v sites than OH species at the O sites. Very recently, Schweke et al.^[13] using thermal gravimetric analysis and thermal desorption spectroscopy of ceria powders studied the influence of temperature, hydrogen partial pressure, and oxygen vacancies on the H₂–CeO₂ interaction. The presence of oxygen vacancies was found to lead to the penetration of hydrogen into the sub-surface and bulk, possibly as hydride species.

The likely net chemical reactions between H₂ and ceria include:

homolytic dissociation to OH [Eq. (1)]:



oxygen vacancy formation [Eq. (2)]:



homolytic dissociation to Ce–H [Eq. (3)]:



heterolytic dissociation [Eq. (4)]:



It is clear that the H₂–CeO₂ interaction is complex and quite sensitive to the reaction conditions. Combined studies on model systems with different levels of complexity have been demonstrated to be an effective strategy towards a fundamental understanding of complex systems.^[14] Herein, we report a comprehensive experimental study of H₂ interaction with well-defined CeO₂(111) thin films and CeO₂ powders in wide range of temperatures and pressures, combined with DFT calculations of CeO₂(111) surfaces with oxygen vacancies at the surface and in the bulk. We provide spectroscopic evidence for the interplay between hydroxyl and hydride formation within the bulk, and connect those results to the evidence presented for the corresponding species on the surface and in the near surface region, allowing us to reach a consistent picture.

Results and Discussion

Ceria thin films

We first address experimental results obtained on the fully stoichiometric CeO₂(111) thin films using infrared reflection absorption spectroscopy (IRAS) and X-ray photoelectron spectroscopy (XPS). Figure 1a shows a series of IRAS spectra measured in 10 mbar of D₂ at several temperatures in the range of 300–600 K. No reaction occurs at 300 K. On the sample exposed to D₂ at 400 K (henceforth denoted as “CeO₂-400”), D₂ dissociates forming OD species identified by the ν(OD) band at about 2700 cm⁻¹ depending on exposure (see Figure S1 in Supporting Information). Upon cooling to 235 K in D₂ atmosphere, the band increases in intensity and shifts to the higher wavenumbers. Interestingly, this band disappears after pumping D₂ out.

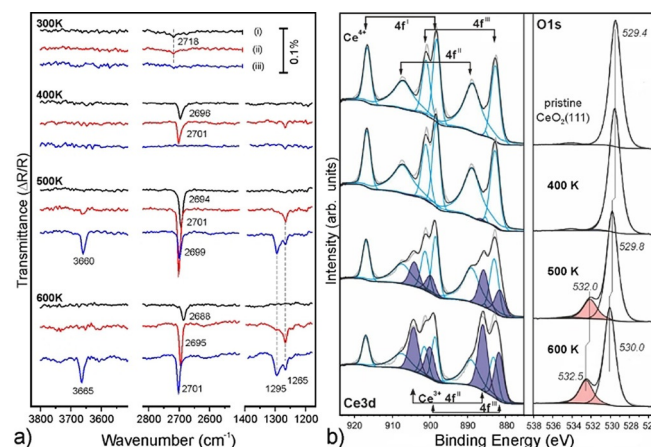


Figure 1. a) IRAS spectra measured on a CeO₂(111) film in 10 mbar of D₂ at the indicated temperature (i); after sample cooling to 235 K (ii); and after subsequent pumping of the D₂ gas phase and heating to 300 K (iii). ν(OH), ν(OD), and ν_{sym}(CO₂) regions are shown. b) Ce 3d and O 1s XPS spectra measured at grazing emission (60° off-normal) for CeO₂(111) films as grown and after D₂ exposure at three different temperatures as indicated. The spectral deconvolution is highlighted.

However, it only decreases in intensity on the “CeO₂-500” sample while the intensity remains on the “CeO₂-600” sample, thus indicating different stability of surface ODs formed at different adsorption temperatures. Concomitantly, the $\nu(\text{OH})$ bands at 3660 and 3665 cm⁻¹ and additional bands at 1295 and 1265 cm⁻¹ emerge, which are assigned to adventitious adsorption of residual H₂O and CO₂ from the vacuum background.

To examine whether the reaction with hydrogen induced changes in the electronic structure, we measured XPS spectra immediately after the IRAS measurements. The spectra of the Ce 3d and O 1s core levels were recorded both at normal and grazing emissions, the latter are only shown in Figure 1 b. The complex Ce 3d spectra in CeO₂ are usually rationalized in terms of the spin orbit pairs of the Ce3d⁹4f⁰O2p⁶, Ce3d⁹4f¹O2p⁵ and Ce3d⁹4f²O2p⁴ final states,^[15] labeled in the Figure as 4f', 4f'' and 4f''', respectively. If present, Ce³⁺ species manifest themselves by additional signals, which correspond to the 4f'' and 4f''' final states. Since the Ce⁴⁺ and Ce³⁺ states overlap, the degree of ceria reduction can only be determined after a relatively complex deconvolution procedure and background subtraction.

The fully stoichiometric CeO₂(111) films exhibited a Ce³⁺/(Ce³⁺ + Ce⁴⁺) signal ratio (henceforth, Ce³⁺ concentration) of about 0.01. After reaction with D₂ at 300 and 400 K, no additional Ce³⁺ species were detected, suggesting that surface reduction does not occur at low temperatures, in full agreement with the IRAS results. In contrast, considerable amounts of Ce³⁺ are observed after reactions at 500 and 600 K, indicating progressive ceria reduction at high temperatures. A well-resolved O1s signal at the higher binding energy (BE) side of the main peak at 529.4 eV is assigned to OH(OD) and carbonates-like species detected by IRAS (Figure 1 a).

It is important to note that, upon increasing the D₂ exposure temperature from 500 to 600 K, the intensity of the adsorbates-related O 1s signal, normalized to the total O 1s signal, only slightly increases, from 0.18 (0.09) to 0.22 (0.1) measured at grazing (normal) emission, whereas the Ce³⁺ concentration measured from analysis of the Ce 3d region increases substantially, from 0.28 (0.16) to 0.55 (0.42). This finding indicates that, after the reaction at 600 K, considerable amounts of oxygen vacancies are located not only at the surface (where they would be easily filled by residual water as shown by IRAS), but also in the sub-surface region.

In the next set of experiments, we addressed interaction of D₂ with reduced, i.e., CeO_{2-x}(111) film surfaces. Figure 2a summarizes the IRAS results of the exposure experiments at different temperatures. Note that, in contrast to the CeO₂(111) surface, the reduced surface may react with traces of water in the UHV background even before the introduction of D₂, thus forming OH species as shown in spectra marked by (*) for three different temperatures. The corresponding XPS results are displayed in Figure 2b.

The results of experiments with D₂ at 300 K nicely reproduce our previous results obtained with H₂.^[12] No surface ODs are observed upon D₂ exposure, whereas XPS (not shown here) revealed a strong electronic effect: Almost no Ce³⁺ remained at

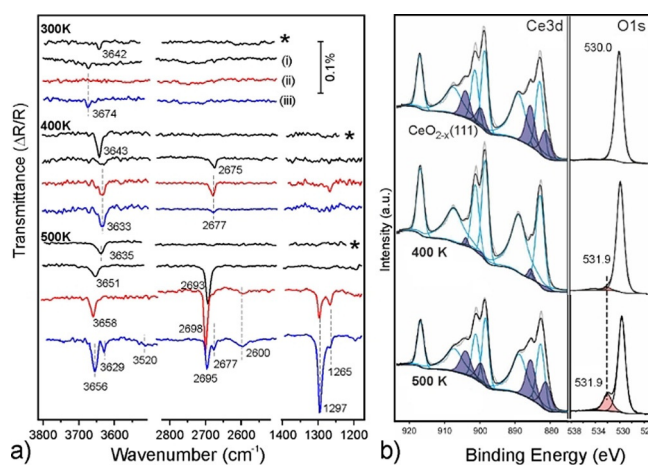


Figure 2. a) IRAS spectra recorded on reduced CeO_{2-x}(111) films in 10 mbar of D₂ at the indicated temperature (i); after sample cooling to 235 K in D₂ (ii); and after subsequent pumping out of the D₂ gas phase and heating to 300 K (iii). Spectra recorded at 300 K prior to the D₂ exposure are marked by (*). b) Ce 3d and O 1s XPS spectra measured at grazing emission (60° off-normal) for reduced CeO_{2-x}(111) films as grown and after D₂ exposure at two different temperatures indicated. The spectral deconvolution is highlighted.

the surface after D₂ treatment indicating the formation of Ce⁴⁺-D⁻ species.

At 400 K, D₂ dissociates giving rise to a weak $\nu(\text{OD})$ band at 2675 cm⁻¹. Upon cooling in D₂, the band gains in intensity together with the OH band (from residual water). After pumping the D₂ gas phase out and then heating the sample to 300 K, the OH band increases at the expense of the OD band. However, the measured frequency ratio ($\nu(\text{OH})/\nu(\text{OD}) = 1.357$) suggests that OH and OD species are identical in nature, thus occupying the same adsorption sites. The interplay between intensities of OH and OD bands can be explained by the H-D exchange reaction and/or by competition between H₂O and D₂ for adsorption sites.

Again, after reaction at 400 K, the Ce³⁺ concentration is dramatically decreased (Figure 2b) due to the formation of hydride species. Small amounts of Ce³⁺ originate from surface hydroxyl species, detected by IRAS (Figure 2a) and O1s XPS. Since the integral intensity of the O1s signal remains unchanged after reaction, the observed oxidation of ceria cannot be explained by migration, if any, of lattice O from deeper layers to the surface. Therefore, the interaction of hydrogen with reduced ceria surfaces at 300 and 400 K primarily results in hydride species.

The same experiment at 500 K, however, revealed a different picture. While also here the adsorption of residual H₂O gives rise to a $\nu(\text{OH})$ band at 3635 cm⁻¹, surface hydroxylation through D₂ dissociation dominates the spectra: A strong $\nu(\text{OD})$ band appears at 2693 cm⁻¹. Upon subsequent cooling and pumping, a weak band emerges around 2600 cm⁻¹, which falls in the range of frequencies characteristic for H-bonded hydroxyls,^[16] and additional bands appear in both the $\nu(\text{OH})$ and $\nu(\text{OD})$ regions, i.e., at 3629 and 2677 cm⁻¹, respectively. These latter values closely resemble those observed in experiments

at 400 K, and probably develop during the reaction while sample cooling in D_2 atmosphere.

In contrast to the experiments at 300 and 400 K, comparison of the Ce3d spectra before and after reaction with D_2 at 500 K revealed similar concentration of Ce^{3+} . However, a significant portion of Ce^{3+} species may originate from a high density of surface hydroxyls, which obscure XPS detection of hydride species. It may also well be that H(D) atoms migrate into the deeper layers of ceria at 500 K and thus become “invisible” to surface sensitive XPS. Both the Ce3d and O1s spectra after reaction at 500 K look virtually identical to those obtained during the same experiment on the stoichiometric $CeO_2(111)$ film (Figure 1b). Even IRAS spectra measured on CeO_2 and CeO_{2-x} films at 500 K in D_2 atmosphere display almost identical intensity and position of $\nu(OD)$ bands (Figure 3a). Based on these results, one concludes that the initial degree of surface reduction does not play a critical role in the D_2 - CeO_2 interaction at elevated temperatures, since the surface reduction and oxygen vacancy formation occurs in situ on the initially oxidized ceria surface via recombinative desorption of surface hydroxyls formed by hydrogen dissociation.

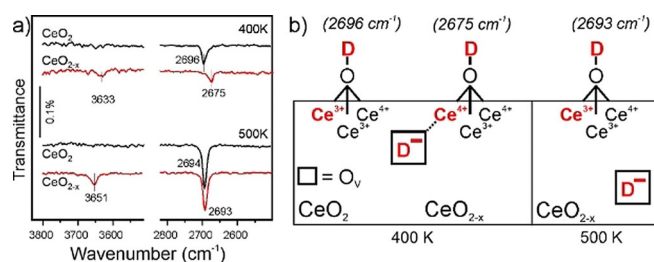


Figure 3. a) Comparison of IRAS spectra measured on $CeO_2(111)$ and $CeO_{2-x}(111)$ films in 10 mbar of D_2 at 400 K and 500 K. b) Schematic representation of D species formed on oxidized (CeO_2) and pre-reduced (CeO_{2-x}) surfaces.

It is interesting that the position of the OD bands observed on CeO_2 and CeO_{2-x} films at 400 K show considerably different frequencies, i.e., 2696 and 2675 cm^{-1} , respectively (see Figure 3a). To rationalize this result, we refer to DFT calculations^[11] showing that the frequency depends on the local degree of reduction surrounding the surface hydroxyl, i.e., on the number of Ce^{3+} ions among the three Ce ions the hydroxyl is coordinated to: The higher the Ce^{3+} ion content, the higher the frequency. Therefore, the OD groups formed on the fully oxidized CeO_2 surface (2696 cm^{-1}) are coordinated to more reduced Ce ions than the OD groups formed on the pre-reduced CeO_{2-x} surface (2675 cm^{-1}) (see Figure 3b for a schematic representation). Even though this might be counterintuitive, the effect can be explained if we recall the XPS results (Figure 2b) showing that the D_2 interaction with the reduced CeO_{2-x} surface at 400 K results in hydride species and the oxidation of Ce^{3+} to Ce^{4+} . Therefore, the low-frequency band may be assigned to OD which is coordinated to Ce–D hydride species formed on the reduced films (Figure 3b). Such a red-shift could even be used as an indication for hydride species at the surface. In the same manner, the low-frequency “satellite” bands (3629 and

2677 cm^{-1}) found for the CeO_{2-x} surface treated at 500 K (Figure 2a) can also be assigned to OH and OD groups on surface hydride sites, which are formed during sample cooling in D_2 .

Therefore, combined IRAS and XPS study on well-defined $CeO_2(111)$ films shows that molecular hydrogen dissociates at relatively high pressures and temperatures and forms surface hydroxyls. On pre-reduced films, however, both surface hydroxyls and hydrides are formed. The hydride formation seems to be the favorable process at relatively low temperatures (< 400 K) within the surface layers probed by XPS, while hydroxylation dominates at higher temperatures, which is accompanied by surface reduction through water desorption.

Ceria powders

Now we address experimental results for the H_2 - CeO_2 interaction obtained on ceria powders under realistic pressure conditions, i.e., 1 atm 5% H_2/He , 1 atm H_2 , and 10 atm H_2 , in order to investigate the interplay between surface and bulk in hydroxyl and hydride formation. As shown by electron microscopy (Figure 4), conventional CeO_2 powders (from Sigma–Aldrich, see Supporting Information) consist of irregularly shaped polyhedral nanoparticles (10–50 nm) which primarily expose the (111) facets and minor (110) and (100) facets.^[3b,c,17] This morphology basically remains after CeO_2 powders were treated in 1 atm of H_2 at 773 K. Since it has been shown by DFT calculations,^[9] that the energies to create oxygen vacancies on the (111), (100) and (110) surfaces are comparable (i.e., 2.0–2.6 eV), and all are much smaller than in the bulk (3.4 eV), the comparison between the powder samples and the $CeO_2(111)$ thin films appears to be appropriate.

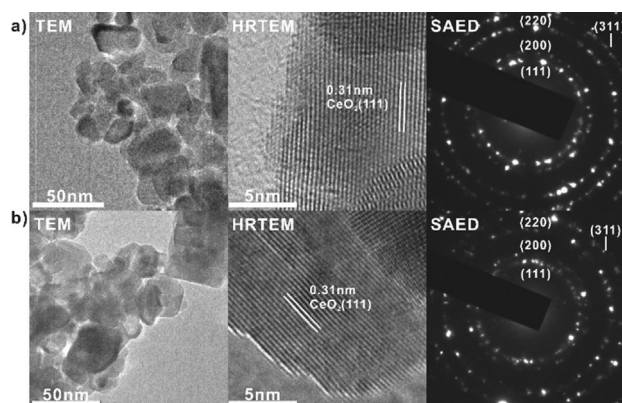


Figure 4. TEM and HRTEM images and SAED patterns of ceria powders before (a) and after (b) treatment in 1 atm of H_2 at 773 K.

According to the temperature programmed reduction (TPR) spectra (Figure S2), surface reduction in 1 atm of 5% H_2/He commences at above 500 K.^[8b] In pure H_2 , the reduction reasonably occurs at lower temperatures (≈ 380 K) and reaches a maximum at 440 K. Hydrogen uptake peak at 615 K is associated with the reduction in subsurface/bulk region.^[8b] Both processes are accompanied by the formation of water. It appears that the reduction of ceria becomes more difficult with increas-

ing H₂ pressure to 10 atm. A broad water signal peaked at 522 K may be attributed to reduction both at surface and in subsurface/bulk layers. Meanwhile, the H₂ consumption does not occur concurrently with the water production, beginning already at 360 K and maximizing at 470 K. These observations suggest that the interaction with hydrogen at 10 atm occurs at profoundly lower temperatures that, in turn, influences the subsequent reduction of ceria.

Figure 5a shows *in situ* diffuse reflectance infrared Fourier transform spectroscopy (DRIFTS) spectra of ceria powders exposed to H₂ at various conditions. (Henceforth, the notation CeO_{2-x}-X-Y stands for ceria treated in X atm of H₂ and temperature Y (in K).) In the ν(OH) region, a vibrational feature at 3666 cm⁻¹ emerges upon exposure to 1 atm H₂ at 473 K, which grows and shifts to 3655 cm⁻¹ at 723 K. In addition, a new broad band centered at 950 cm⁻¹ appears. (Weak vibrational features at 860, 1016 and 1044 cm⁻¹ in this region arise from adventitious CO₂ adsorption.^[18]) The spectrum does not change much in 10 atm of H₂ at 723 K. Moreover, the observed bands are stable and basically remain after sample cooling to 373 K and subsequent pumping the H₂ gas out (Figure S3). Ceria exposed to 10 atm D₂ at 723 K revealed a strong OD band at 2691 cm⁻¹, which corresponds to the OH counterpart at 3655 cm⁻¹ in the H₂ experiments, and nicely matches the one observed by IRAS on the ceria films at 500–600 K (see Figures 1a and 2a). The 950 cm⁻¹ band disappears upon D₂ adsorption, indicating that this feature relates to the H-involving vibrations. This band falls in the range of frequencies characteristic for vibrations of bulk Ce–H species.^[10,19] Accordingly, Ce–D species would show up at frequencies strongly red-shifted as compared to Ce–H, which is below the cut-off frequency of our setups (both for IRAS studies on thin films and DRIFT studies on powders). Please note, that IRAS spectra on metal supported films obey the well-known metal selection rules^[20] and detect only vibrations associated with dipole changes normal to the surface. Therefore, our present results provide first IR-based experimental evidence for the formation of bulk hydride species upon interaction with H₂. A relatively large bandwidth indicates the presence of Ce–H in different local environments. In addition to bulk species, the surface Ce–H

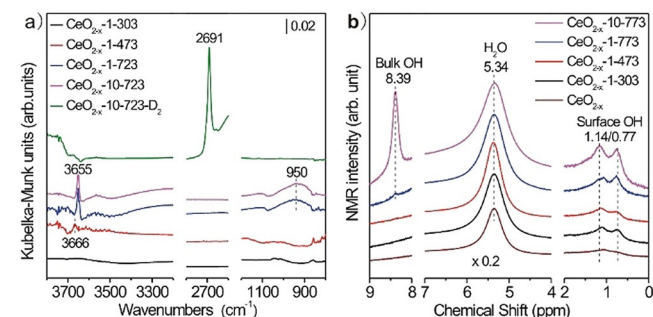


Figure 5. a) *In situ* DRIFTS spectra measured for ceria treated in H₂ at different conditions and in 10 atm D₂ at 723 K. The spectra measured on ceria samples treated in Ar at 723 K and cooled to specified temperatures were used as the references. b) MAS ¹H NMR spectra measured for ceria treated in H₂ at different conditions and then cooled in H₂ to room temperature.

species was previously observed in oxidized ceria rods exposed to 1 bar H₂ at 673 K, which exhibited a vibrational feature at around 500 cm⁻¹ in inelastic neutron scattering spectra.^[10] Note also that the indications of Ce–H vibrations in a very recent Raman study of cerium-hydride growth centers on metallic Ce foil.^[21]

Figure 5b displays respective MAS ¹H NMR spectra of the H₂-treated ceria samples. Unfortunately, Ce–H species cannot be detected.^[22] Ceria heated at 773 K in He exhibits signals at 1.14/0.77 and 5.34 ppm arising from surface OH groups and adsorbed H₂O, respectively.^[23] The signals grow with the H₂ pressure and temperature. An additional weak feature emerges at 8.39 ppm upon exposure to 1 atm H₂ at 773 K and increases significantly upon exposure to 10 atm H₂ at 773 K. This feature can be assigned to bulk OH groups in ceria.^[23] Therefore, the NMR results provide clear evidence of the increase of the total OH coverage. The OH formation mainly occurs on the surface at temperatures up to 473 K and extends to the bulk region at 773 K. Comparing the evolutions of bulk Ce–H species derived from the *in situ* DRIFTS results and bulk OH group from the NMR results, we infer that the formation of bulk Ce–H species is more favored than that of bulk OH groups in ceria exposed to H₂ at 773 K, where bulk reduction occurs and bulk oxygen vacancies form. (The full dataset of DRIFTS and NMR results are shown in Figures S4 and S5.)

In order to link these results to the thin film data, the ceria samples were characterized by XPS (Figure 6a and Figures S6a, S7). Based on XPS data, ceria heated to 773 K in He, in order to create oxygen vacancies, exhibits an initial Ce³⁺ concentration of 9.2% within the near surface region determined by the escape depth of the Ce 3d-electrons (≈3 nm), henceforth referred to as Ce³⁺_{surf}. Then, the sample was exposed to 1 atm H₂ at three different temperatures (303, 473, and 773 K). Consequently, those samples were annealed at the elevated temperatures, up to 773 K, and XPS spectra were recorded. Exposure to 1 atm of H₂ at room temperature (CeO_{2-x}-1-303) decreases the Ce³⁺_{surf} concentration, as also observed above for

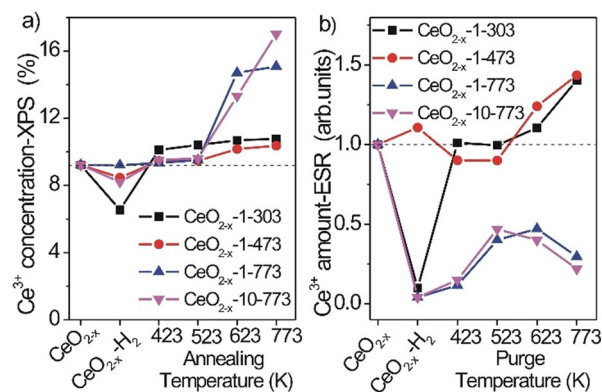


Figure 6. a) Ce³⁺_{surf} concentration derived from XPS and b) changes in the Ce³⁺_{bulk} concentration (normalized to pristine ceria) derived from EPR, for ceria samples treated in H₂ at different conditions and then cooled in H₂ to room temperature followed by vacuum annealing (for 30–60 min) during XPS measurements or purging in He (for 2 hours) during ESR measurements at indicated temperatures.

the films, due to OH and hydride formation and its interconversion. Increase in temperature under the same pressure conditions (CeO_{2-x} -1-473, CeO_{2-x} -1-773), or in pressure at 773 K (CeO_{2-x} -10-773), leads to a smaller effect. Upon vacuum annealing of the samples the amount of $\text{Ce}^{3+}_{\text{surf}}$ increases due to water desorption and shows the biggest effect for the sample treated at 10 atm.

Now we compare the XPS results with EPR data (spectra are shown in Figures S6b and S8), probing both surface/near surface and bulk species. The relative changes in the Ce^{3+} concentration (henceforth, $\text{Ce}^{3+}_{\text{bulk}}$), as represented by the EPR intensity normalized to that of pristine ceria (prepared in the same way as the samples for XPS), are shown in Figure 6b. Except the CeO_{2-x} -1-473 sample, the $\text{Ce}^{3+}_{\text{bulk}}$ concentration drops to very low values in CeO_{2-x} -1-773 and CeO_{2-x} -10-773, as well as for the room temperature sample, clearly indicating bulk hydride formation in these samples. Since EPR probes the entire sample, both surface and bulk, the small amount of Ce^{3+} near the surface (monitored by XPS, Figure 6a) contributes much less to the signal. The obvious increase of Ce^{3+} observed by XPS and EPR on the CeO_{2-x} -1-303 sample upon vacuum annealing or purging at 423 K reflects the transformation of surface Ce^{4+}H^- into more stable surface OH, accompanied by the reduction of Ce^{4+} into Ce^{3+} , and the decomposition of surface $\text{CeO}_v^{4+}\text{H}^-$ into hydrogen and CeO_v^{3+} .^[12] It is interesting to note, that, after He purging at and above 423 K, the EPR data for the CeO_{2-x} -1-303 almost match the set of data taken on the CeO_{2-x} -1-473 sample. A glance at the water desorption data (Figure S9) tells us that this is due to the onset of water desorption and thus oxygen vacancy formation around 400 K. Both the $\text{Ce}^{3+}_{\text{surf}}$ and $\text{Ce}^{3+}_{\text{bulk}}$ concentrations in CeO_{2-x} -1-303 and CeO_{2-x} -1-473 and the $\text{Ce}^{3+}_{\text{surf}}$ concentrations in CeO_{2-x} -1-773 and CeO_{2-x} -10-773 then increase and exceed the initial concentration of CeO_{2-x} upon vacuum annealing or purging at 523 K and above, again, mainly due to the recombinative reaction of surface OH groups to produce water and create O_v and Ce^{3+} . However, the $\text{Ce}^{3+}_{\text{bulk}}$ concentrations in the CeO_{2-x} -1-773 and CeO_{2-x} -10-773 samples are always lower than the initial concentration, indicating the presence of bulk Ce–H species. They increase upon annealing at 523–623 K via the reaction $2\text{CeO}_v^{4+}\text{H}^- \rightarrow \text{H}_2(\text{g}) + 2\text{CeO}_v^{3+}$, but decrease at higher temperatures (773 K), although the H_2 production continues (Figure S9). On one hand, this agrees with the DRIFTS results that the H_2 productions above 623 K for CeO_{2-x} -1-773 and CeO_{2-x} -10-773 involve the OH species. On the other hand, this indicates the re-formation of bulk $\text{CeO}_v^{4+}\text{H}^-$ species most likely by the migration of H atoms in surface OH species to bulk CeO_v^{3+} sites. Similar phenomena were previously observed to occur on the highly hydrogenated and reduced TiO_2 surfaces.^[24] These observations demonstrate that the stability of Ce–H species enhances greatly with the O_v concentration in ceria.

In summary, the variations of $\text{Ce}^{3+}_{\text{surf}}$ and $\text{Ce}^{3+}_{\text{bulk}}$ species (determined by XPS and EPR, respectively) indicate relative amounts of Ce^{3+} created by the homolytic dissociation to OH and oxygen vacancy formation reactions [Eqs. (1) and (2) in the Introduction], and annihilated by the homolytic dissociation to

$\text{CeO}_v^{4+}\text{H}^-$ [Eq. (3)], which, together with the formed H species, can be used to deduce which reactions occur upon H_2 – CeO_2 interaction and where. Certainly, the $\text{Ce}^{3+}_{\text{surf}}$ and $\text{Ce}^{3+}_{\text{bulk}}$ species overlap in the subsurface region. Compared to ceria pre-treated at 773 K in He, the CeO_{2-x} -1-303 sample contains less $\text{Ce}^{3+}_{\text{surf}}$ and $\text{Ce}^{3+}_{\text{bulk}}$ due to the kinetically-favored heterolytic dissociation to OH and Ce^{4+}H^- on the ceria surface [Eq. (4)] and homolytic dissociation to $\text{CeO}_v^{4+}\text{H}^-$ at surface oxygen vacancy sites [Eq. (3)]. At 473 and 773 K, H_2 undergoes the thermodynamically favored homolytic dissociation to OH species on the ceria surface, the oxygen vacancy formation reaction, and the homolytic dissociation to $\text{CeO}_v^{4+}\text{H}^-$ at initially present and newly formed oxygen vacancies in the sub-surface region, leading to almost unchanged $\text{Ce}^{3+}_{\text{surf}}$ as initially observed in CeO_{2-x} -1-473, CeO_{2-x} -1-773 and CeO_{2-x} -10-773. The only slightly increased $\text{Ce}^{3+}_{\text{bulk}}$ concentration observed for CeO_{2-x} -1-473 is likely due to either limited creation of bulk oxygen vacancies or the limited diffusivity of hydride filled oxygen vacancies at that temperature. However, CeO_{2-x} -1-773 and CeO_{2-x} -10-773 with high oxygen vacancy concentrations, arising either from diffusion or creation in the bulk, exhibit almost no $\text{Ce}^{3+}_{\text{bulk}}$, indicating the formation of bulk $\text{CeO}_v^{4+}\text{H}^-$. Those samples also exhibit bulk OH species arising from the homolytic dissociation to OH or the heterolytic dissociation in the bulk.

Theoretical calculations

To study the relative stabilities of proton (H^+ –O) and hydride (H^- –Ce) species at $\text{CeO}_2(111)$ surfaces with different degrees of reduction, we constructed $\text{CeO}_2(111)\text{-}n\text{OV}_{\text{surf}}$ [n refers to the number of surface oxygen vacancies ranging from 1 to 4, and $n = 4$ corresponds to a O_v coverage of 0.16 monolayer (ML)] based on the “hydroxyl-vacancy model”.^[25] Note that for the cases of $n = 2, 3$, and 4, the surface oxygen vacancies form an energetically favorable (linear) surface oxygen vacancy dimer, trimer, and tetramer, respectively (Figure 7a). It can be seen from Figure 8a that, by increasing the concentration of surface oxygen vacancies ($n = 1 \rightarrow 4$), the adsorption energy (strength) of proton decreases significantly (1.40 \rightarrow 0.61 eV), which agrees well with the previous theoretical study.^[26] In contrast, the adsorption energy of hydride shows an opposite trend. More specifically, the adsorption energy of hydride drastically changes from -0.71 to 0.41 eV, when increasing the concentration of surface oxygen vacancies ($n = 1 \rightarrow 4$), indicating that surface hydride can be stabilized by oxygen vacancies. Presumably, this is because the electron-donating character of $\text{CeO}_2(111)$ is enhanced, and, hence, surface hydride gets stabilized. Therefore, it may be expected that surface hydride is more stable than surface hydrogen atom at heavily reduced $\text{CeO}_2(111)$ surfaces with $n > 4$, although we were not able to simulate such surfaces due to the high computational cost.

We also evaluated the relative stabilities of hydrogen atom and hydride species in the bulk of ceria by constructing the slab models of $\text{CeO}_2(111)$ with one and four aggregated oxygen vacancies in the middle O–Ce–O trilayer (denoted as $\text{CeO}_2(111)\text{-}1\text{OV}_{\text{bulk}}$ and $\text{CeO}_2(111)\text{-}4\text{OV}_{\text{bulk}}$, respectively, see Figure 7b). Not surprisingly, compared with the surface case,

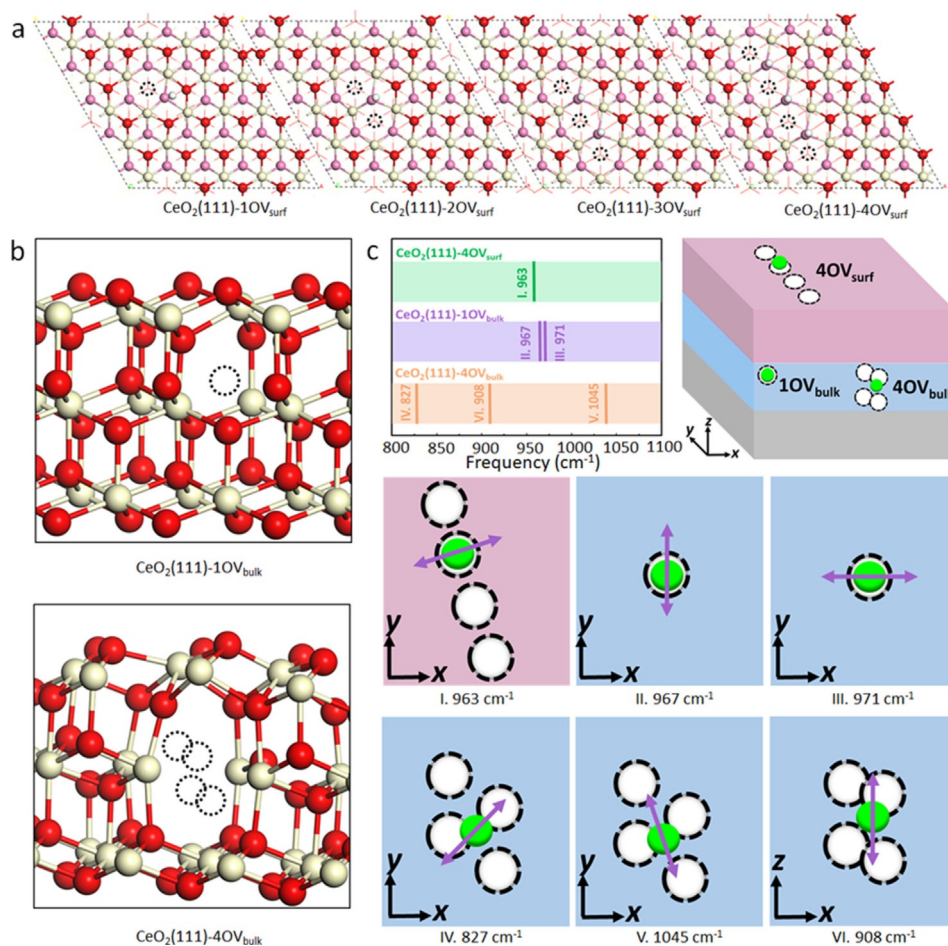


Figure 7. a) Optimized structures (top view) of CeO₂(111)-*n*OV_{surf} (*n* = 1, 2, 3, or 4). Surface cerium, hydrogen, surface oxygen, and subsurface oxygen atoms are represented by light yellow, white, red, and pink balls, respectively; the bottom two O-Ce-O trilayers are drawn with lines for clarity. b) Optimized structures (side view) of CeO₂(111)-1OV_{bulk} and CeO₂(111)-4OV_{bulk}. Cerium and oxygen atoms are in light yellow and red, respectively. c) Scaled DFT-calculated vibrational frequencies of surface and bulk hydrides based on the selected models (i.e., CeO₂(111)-4OV_{surf}, CeO₂(111)-1OV_{bulk}, and CeO₂(111)-4OV_{bulk}) and schematic views of the corresponding vibrational modes. The top, middle, and bottom O-Ce-O trilayers of the CeO₂(111) slab are simplified by light red, light blue, and gray sheets, respectively. The purple arrows represent the directions of the vibrations of the hydrides (green balls). In a, b, and c, dashed black circles represent oxygen vacancies.

oxygen vacancies in the “bulk” have similar effects on the stabilities of surrounding hydrogen atom and hydride species (see Figure 8b). It is interesting to note that, for the vacancy-rich case of CeO₂(111)-4OV_{bulk}, the bulk hydride is ≈ 1.4 eV more stable than a corresponding hydrogen atom, suggesting that hydride is the dominant species in the bulk region of heavily reduced ceria. Meanwhile, these results also indicate, that bulk hydride is more stable than surface hydride, whereas a surface hydrogen atom is more stable than a bulk hydrogen atom.

Based on the representative CeO₂(111)-4OV_{surf} model, we studied the following three possible dissociation pathways of H₂: (i) homolytic dissociation of H₂ to two surface hydrogen atoms (denoted as the homolytic-1 pathway); (ii) homolytic dissociation of H₂ to two surface hydrides (the homolytic-2 pathway); (iii) heterolytic dissociation of H₂ to one surface proton and one surface hydride (the heterolytic pathway). The calculated energy profiles and the relevant structures are presented in Figure 8c and Figure S12, respectively. The three dissociation pathways all start from a weakly adsorbed H₂ (*E*_{ads} = 0.02 eV)

above a Ce atom. We found that the heterolytic pathway gives the lowest activation energy barrier of 0.56 eV, followed by the homolytic-2 pathway (barrier: 1.15 eV). Although the homolytic-1 pathway is thermodynamically most favorable, it has a highest barrier of 1.75 eV, which is consistent with the previous study.^[7b] Therefore, formation of surface hydride through the heterolytic and homolytic-2 pathways is kinetically favorable on the CeO₂(111)-4OV_{surf} surface. We also found that the transformation of surface hydride to surface proton is extremely difficult at CeO₂(111)-4OV_{surf} since it needs to overcome a high barrier of 2.67 eV (Figure 8d and Figure S13). Accordingly, hydride is kinetically stable at such surface. Meanwhile, the recombinative desorption of surface hydrides to H₂ is most favorable both, thermodynamically and kinetically, among all H₂ production pathways from H species. The results based on the CeO₂(111)-4OV_{surf} and CeO₂(111)-4OV_{bulk} models also suggest that surface hydrides, once formed, can readily diffuse into the bulk region and be stabilized therein at heavily reduced conditions. Therefore, the DFT results fully agree with the above experimental observations for H₂-CeO_{2-x} powder systems.

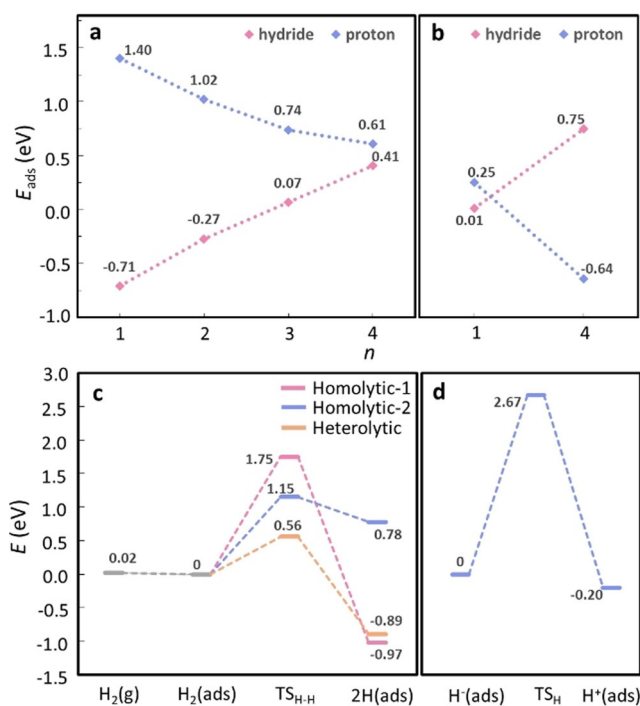


Figure 8. Calculated adsorption energies (E_{ads}) of hydride and proton as a function of the number of oxygen vacancies based on a) $\text{CeO}_2(111)-n\text{OV}_{\text{surf}}$ ($n = 1, 2, 3, \text{ or } 4$) and b) $\text{CeO}_2(111)-n\text{OV}_{\text{bulk}}$ ($n = 1 \text{ or } 4$). Calculated energy profiles for c) H_2 dissociation on $\text{CeO}_2(111)-4\text{OV}_{\text{surf}}$ through the homolytic-1, homolytic-2, and heterolytic pathways and d) the transformation of surface hydride to surface hydrogen atom on $\text{CeO}_2(111)-4\text{OV}_{\text{surf}}$. For c, $\text{H}_2(\text{g})$, $\text{H}_2(\text{ads})$, $\text{TS}_{\text{H-H}}$, $2\text{H}(\text{ads})$ represent, respectively, the state with gas-phase H_2 , the surface adsorption state of H_2 , the transition state of H_2 dissociation, and the surface adsorption state of two H (which can be hydride or hydrogen atom). For d, $\text{H}^-(\text{ads})$, TS_{H} , and $\text{H}^+(\text{ads})$ represent, respectively, the surface adsorption state of hydride, the transition state of transformation of hydride to proton, the surface adsorption state of proton. Corresponding structures are shown in Figures S10–S13.

The scaled DFT-calculated vibrational frequencies of surface and bulk hydrides based on the selected models (i.e., $\text{CeO}_2(111)-4\text{OV}_{\text{surf}}$, $\text{CeO}_2(111)-10\text{V}_{\text{bulk}}$, and $\text{CeO}_2(111)-4\text{OV}_{\text{bulk}}$) are summarized in Table S1. The vibrations of bulk hydride depend strongly on the configuration of oxygen vacancies, but they cover the experimentally observed broad vibrational band centered at 950 cm^{-1} (Figure 7c). For surface hydride, the vibration at 963 cm^{-1} (Figure 7c) exhibits a dipole moment parallel to the surface, which rationalizes its absence in IRAS experiments with $\text{CeO}_{2-x}(111)$ thin film due to the well-known metal surface selection rule applied in IRAS.^[20]

Summary

Our combined experimental and computational results provide a comprehensive picture of the H_2 -ceria interaction and highlight the vital role of oxygen vacancies in this process as well as the important interplay between surface and bulk. On a stoichiometric CeO_2 surface, H_2 only dissociates to form surface hydroxyls at elevated temperatures. On reduced CeO_{2-x} hydroxyls and hydrides are formed on the surface and in the bulk, depending on O_v concentration and location. The general

trends are that hydroxyl is destabilized as the O_v coverage increases, whereas hydride is stabilized, and that surface hydroxyl is more stable than bulk hydroxyl, whereas bulk hydride is more stable than surface hydride. The surface hydride formation is the kinetically favorable process at relatively low temperatures, and the resulting surface hydride can easily diffuse into the bulk region and get stabilized therein. At higher temperatures, surface hydroxyls can react to produce water and create additional oxygen vacancies, which in turn control the H_2 -ceria interaction.

The results demonstrate the facile formation of hydride ($\text{Ce}_{\text{Ov}}^{4+}\text{H}^-$) at the $\text{Ce}_{\text{Ov}}^{3+}$ site, leading to the oxidation of $\text{Ce}_{\text{Ov}}^{3+}$. Ce^{3+} sites associated with oxygen vacancies play an important role in determining the CeO_{2-x} reactivity, therefore, their annihilation via the $\text{Ce}_{\text{Ov}}^{4+}\text{H}^-$ formation will affect the CeO_{2-x} reactivity. The results also demonstrate the hydride formation at the in situ created oxygen vacancy sites of ceria during the reduction process, suggesting that the ceria reduction by H_2 should follow the reaction equation $\text{CeO}_2 + (x+y)\text{H}_2 \rightarrow \text{CeO}_{2-x} + x\text{H}_2\text{O} + 2y\text{Ce}_{\text{Ov}}^{4+}\text{H}^- + (x-y)\text{O}_v$, rather than $\text{CeO}_2 + x\text{H}_2 \rightarrow \text{CeO}_{2-x} + x\text{H}_2\text{O} + x\text{O}_v$.

We believe that our results showing the diversity of reaction pathways taking place upon interaction of H_2 with ceria will aid in full understanding of the reactivity of ceria-based catalysts in a hydrogen-rich atmosphere.

Acknowledgements

This work is financially supported by National Key R&D Program of MOST (2017YFB0602205), the DFG-NSFC joint project (Nos. FR554/18-1 and 21761132005), the National Natural Science Foundation of China (91945301, 21525313, 91745202, U1930203, 21825301), the Chinese Academy of Sciences, and the Changjiang Scholars Program of Ministry of Education of China. H.J.F. thanks Fonds der Chemischen Industrie. J.Q.Z. thanks the AvH Foundation for a fellowship. Open access funding enabled and organized by Projekt DEAL.

Conflict of interest

The authors declare no conflict of interest.

Keywords: ceria · density functional calculations · hydride · hydrogenation · surface structure

- [1] a) Z. Paál, P. G. Menon, *Hydrogen Effects in Catalysis: Fundamentals and Practical Applications*, Marcel Dekker, New York, **1988**; b) T. Norby, M. Widerøe, R. Glöckner, Y. Larring, *J. Chem. Soc. Dalton Trans.* **2004**, 3012–3018; c) R. Mäs-Balleste, A. Lledos, in *Comprehensive Inorganic Chemistry II: From Elements to Applications, Vol. 9* (Eds.: J. Reedijk, K. Poeppelemer), Elsevier, Oxford, **2013**, p. 727.
- [2] a) V. E. Henrich, P. A. Cox, *The Surface Science of Metal Oxides*, Cambridge University Press, Cambridge, **1994**; b) J. L. G. Fierro, *Metal Oxides: Chemistry and Applications*, CRC, Boca Raton, **2006**; c) C. Copéret, D. P. Estes, K. Larmier, K. Searles, *Chem. Rev.* **2016**, *116*, 8463–8505.
- [3] a) G. Vilé, B. Bridier, J. Wichert, J. Pérez-Ramírez, *Angew. Chem. Int. Ed.* **2012**, *51*, 8620–8623; *Angew. Chem.* **2012**, *124*, 8748–8751; b) J. Carrasco, G. Vilé, D. Fernández-Torre, R. Pérez, J. Pérez-Ramírez, M. V. Gandu-

- glia-Pirovano, *J. Phys. Chem. C* **2014**, *118*, 5352–5360; c) G. Vilé, S. Colussi, F. Krumeich, A. Trovarelli, J. Pérez-Ramírez, *Angew. Chem. Int. Ed.* **2014**, *53*, 12069–12072; *Angew. Chem.* **2014**, *126*, 12265–12268; d) G. Vilé, P. Dähler, J. Vecchietti, M. Baltanás, S. Collins, M. Calatayud, A. Bonivardi, J. Pérez-Ramírez, *J. Catal.* **2015**, *324*, 69–78; e) T. Cao, R. You, X. Zhang, S. Chen, D. Li, Z. Zhang, W. Huang, *Phys. Chem. Chem. Phys.* **2018**, *20*, 9659–9670; f) T. Cao, R. You, Z. Li, X. Zhang, D. Li, S. Chen, Z. Zhang, W. Huang, *Appl. Surf. Sci.* **2020**, *501*, 144120; g) J. Moon, Y. Cheng, L. L. Daemen, M. Li, F. Polo-Garzon, A. J. Ramirez-Cuesta, Z. Wu, *ACS Catal.* **2020**, *10*, 5278–5287.
- [4] C. Binet, M. Daturi, J.-C. Lavalley, *Catal. Today* **1999**, *50*, 207–225.
- [5] K. Sohlberg, S. T. Pantelides, S. J. Pennycook, *J. Am. Chem. Soc.* **2001**, *123*, 6609–6611.
- [6] a) D. Fernández-Torre, J. Carrasco, M. V. Ganduglia-Pirovano, R. Pérez, *J. Chem. Phys.* **2014**, *141*, 014703; b) F. R. Negreiros, M. F. Camellone, S. Fabris, *J. Phys. Chem. C* **2015**, *119*, 21567–21573; c) M. García-Melchor, N. López, *J. Phys. Chem. C* **2014**, *118*, 10921–10926.
- [7] a) Z.-Q. Huang, L.-P. Liu, S. Qi, S. Zhang, Y. Qu, C.-R. Chang, *ACS Catal.* **2017**, *7*, 546–554; b) C. Riley, S. Zhou, D. Kunwar, A. De La Riva, E. Peterson, R. Payne, L. Gao, S. Lin, H. Guo, A. Datye, *J. Am. Chem. Soc.* **2018**, *140*, 12964–12973.
- [8] a) B. Chen, Y. Ma, L. Ding, L. Xu, Z. Wu, Q. Yuan, W. Huang, *J. Phys. Chem. C* **2013**, *117*, 5800–5810; b) Y. Gao, R. Li, S. Chen, L. Luo, T. Cao, W. Huang, *Phys. Chem. Chem. Phys.* **2015**, *17*, 31862–31871.
- [9] M. Nolan, J. E. Fearon, G. W. Watson, *Solid State Ionics* **2006**, *177*, 3069–3074.
- [10] Z. Wu, Y. Cheng, F. Tao, L. Daemen, G. S. Foo, L. Nguyen, X. Zhang, A. Beste, A. J. Ramirez-Cuesta, *J. Am. Chem. Soc.* **2017**, *139*, 9721–9727.
- [11] K. Werner, X. Weng, F. Calaza, M. Sterrer, T. Kropp, J. Paier, J. Sauer, M. Wilde, K. Fukutani, S. Shaikhutdinov, H.-J. Freund, *J. Am. Chem. Soc.* **2017**, *139*, 17608–17616.
- [12] Z. Li, K. Werner, K. Qian, R. You, A. Plucienik, A. Jia, L. Wu, L. Zhang, H. Pan, H. Kuhlenbeck, S. Shaikhutdinov, W. Huang, H.-J. Freund, *Angew. Chem. Int. Ed.* **2019**, *58*, 14686–14693; *Angew. Chem.* **2019**, *131*, 14828–14835.
- [13] D. Schweke, L. Shelly, R. Ben David, A. Danon, N. Kostirya, S. Hayun, *J. Phys. Chem. C* **2020**, *124*, 6180–6187.
- [14] a) S. Chen, F. Xiong, W. Huang, *Surf. Sci. Rep.* **2019**, *74*, 100471; b) H.-J. Freund, M. Heyde, H. Kuhlenbeck, N. Nilius, T. Risse, Th. Schmidt, S. Shaikhutdinov, M. Sterrer, *Sci. China. Chem.* **2020**, *63*, 426–447.
- [15] D. R. Mullins, *Surf. Sci. Rep.* **2015**, *70*, 42–85.
- [16] a) A. Badri, C. Binet, J.-C. Lavalley, *J. Chem. Soc. Faraday Trans.* **1996**, *92*, 4669–4673; b) S. Bernal, J. J. Calvino, G. A. Cifredo, J. M. Gatica, J. A. P. Omil, J. M. Pintado, *J. Chem. Soc. Faraday Trans.* **1993**, *89*, 3499–3505.
- [17] E. Aneggi, D. Wiater, C. de Leitenburg, J. Llorca, A. Trovarelli, *ACS Catal.* **2014**, *4*, 172–181.
- [18] A. Trovarelli, *Catal. Rev.* **1996**, *38*, 439–520.
- [19] a) A. Fujimori, M. Ishii, N. Tsuda, *Phys. Status Solidi B* **1980**, *99*, 673–681; b) O. Matz, M. Calatayud, *ACS Omega* **2018**, *3*, 16063–16073.
- [20] S. A. Francis, A. H. Ellison, *J. Opt. Soc. Am.* **1959**, *49*, 131–138.
- [21] T. Livneh, D. Avisar, *J. Phys. Chem. C* **2021**, *124*, 28018–28025.
- [22] a) C. Lundin, *Rare Earth Research. Vol. 1*, CRC, **1962**; b) L. Maron, E. L. Werkema, L. Perrin, O. Eisenstein, R. A. Andersen, *J. Am. Chem. Soc.* **2005**, *127*, 279–292.
- [23] L. Gill, A. Beste, B. Chen, M. Li, A. K. Mann, S. H. Overbury, E. W. Hagaman, *J. Phys. Chem. C* **2017**, *121*, 7450–7465.
- [24] a) Z. Wu, F. Xiong, Z. Wang, W. Huang, *Chin. Chem. Lett.* **2018**, *29*, 752–756; b) J. Tao, Q. Cuan, X.-Q. Gong, M. Batzill, *J. Phys. Chem. C* **2012**, *116*, 20438–20446; c) X. L. Yin, M. Calatayud, H. Qiu, Y. Wang, A. Birkner, C. Minot, C. Wöll, *ChemPhysChem* **2008**, *9*, 253–256.
- [25] X.-P. Wu, X.-Q. Gong, *Phys. Rev. Lett.* **2016**, *116*, 086102.
- [26] X.-P. Wu, X.-Q. Gong, G. Lu, *Phys. Chem. Chem. Phys.* **2015**, *17*, 3544–3549.

Manuscript received: December 17, 2020

Accepted manuscript online: December 23, 2020

Version of record online: February 18, 2021